Nano Energy 81 (2021) 105590

Contents lists available at ScienceDirect

Nano Energy

journal homepage: http://www.elsevier.com/locate/nanoen

Full paper

Trampoline inspired stretchable triboelectric nanogenerators as tactile sensors for epidermal electronics

Jiahui He [a,1], Zhaoqian Xie [b,1], Kuanming Yao [a], Dengfeng Li [a], Yiming Liu [a], Zhan Gao [a], Wei Lu [c], Lingqian Chang [d], Xinge Yu [a,*]

[a] Department of Biomedical Engineering, City University of Hong Kong, Hong Kong, China
[b] State Key Laboratory of Structural Analysis for Industrial Equipment, Department of Engineering Mechanics, International Research Center for Computational Mechanics, Dalian University of Technology, Dalian 116024, People's Republic of China
[c] Center for Bio-Integrated Electronics, Northwestern University, Evanston, IL 60208, USA
[d] Key Laboratory for Biomechanics and Mechanobiology of Ministry of Education, Beijing Advanced Innovation Center for Biomedical Engineering, School of Biological Science and Medical Engineering, Beihang University, Beijing 100083, People's Republic of China

ARTICLE INFO

Keywords:
Stretchable electronics
Epidermal electronics
Triboelectric nanogenerator
Tactile sensor
E-skin

ABSTRACT

Recent advances in flexible electronics have brought great promotions to the next generation of wearable devices, like electronic skin (E-skin). Nevertheless, the powering issue still limits the size, weight and cost for E-skin. Here, trampoline inspired mechanics design and processing techniques in epidermal electronics are combined together to develop a thin, soft, stretchable self-powered tactile sensors based on triboelectric effect for E-skin. With the assistance of microstructure modifying by sandpapers, the TENG sensor exhibits great improved electrical performance and capable of distinguishing a broad range of pressure, with a great sensitivity of 0.367 mV Pa^{-1}. The resulted TENG sensor exhibits excellent stretchability and sensing stability with accurate unchanged signal outputs even under a high-level strain up to 35%. Demonstrations of the sensors associating with the integration with a glove for human-machine interfaces and the development of a 4 × 4 tactile array for pressure mapping and recognition of contact objects, offers great opportunity for next generation self-powered E-skin.

1. Introduction

In the field of wearable technologies, there is an increasing demand for ultrathin and soft electronics in various kinds of applications, such as healthcare [1–4], environmental monitoring [5,6] and human-machine interfaces [7–9]. Recent advances in developing intrinsically flexible/stretchable materials [10–16] and employing fancy structural mechanics designs, have been adopted in various kinds of soft devices for sensing of bio-physical and bio-chemical signals i.e. strain [17], temperature [18], humidity [19], blood glucose [20], electrocardiogram (ECG) [21] and electroencephalogram (EEG) [22]. To more accurately sense these information, thin, stretchable and multi-functional sensing platforms that can mimic functionalities of human skin, known as electronic skin (E-skin) has attracted tremendous attention and been thought as the best candidate for artificial skin, since E-skin can be perfectly integrated with body for real-time health monitoring with great accuracy [23–25]. Similarly to traditional electronics, E-skin also requires the integration of numerous sensors and/or actuators, which bring accompanying demands for thin, soft powering systems. Self-powered devices based on various mechanisms such as thermoelectric [26,27], piezoelectric [28], optoelectric [29], magnetoelectric [30] and triboelectric effects [31,32] have been developed into thin soft platforms and thus offer feasible routes to address the soft powering problem. Among these self-powered devices, triboelectric nanogenerators (TENGs) associating with coupling of contact electrification and electrostatic induction enable converting mechanical energy into triboelectricity with simple device architectures but high power conversion efficiencies [33,34]. Moreover, the electrical outputs generated by TENGs can not only provide power supplying for wearable devices, but also offer the opportunity for mechanical forces related sensing such as pressure/tactile detection [35,36]. Given the above advantages, a variety of TENG-based devices have been developed and extensively

* Corresponding author.
E-mail address: xingeyu@cityu.edu.hk (X. Yu).
[1] These authors contributed equally to this work.

https://doi.org/10.1016/j.nanoen.2020.105590
Received 10 September 2020; Received in revised form 6 November 2020; Accepted 6 November 2020
Available online 11 November 2020

extended into diverse applications, i.e. flexible energy harvesting [37], strain/stress sensing [38,39], motion recognition [40,41] and position mapping [42].

Recent advances in engineering materials and devices that used in E-skin have been successfully implanted into TENGs for realizing tactile sensors and energy harvesters. [43–46] However, the development of TENG based self-powered tactile sensors into E-skin is still facing two challenges. First, the stretchability of TENGs is still not as great as epidermal electronics based E-skin that may result in sensing signal unstable under skin deformations, and thus limits the development of TENGs into E-skin formats [46,47]. Second, the signal outputs of TENGs highly depend on the effective working (contact) areas, where most reported TENGs are relatively large with dimension in centimeter or decimeter scales to dilute the electrical crosstalk problems in multiple channels sensor arrays, and therefore limit the applications in high channel counts tactile sensor arrays for high-resolution tactile recognition and mapping [42,48].

Here, we combined structural mechanics designs, microstructure modifying, and transparent shielding layers coating in TENGs, to develop thin, soft, highly stretchable, skin-integrated and crosstalk freed tactile sensors and sensing arrays. Sandpapers severing as molds for microstructures modifying enhanced self-powering efficiency and the resulted self-powered tactile sensors exhibit great sensitivity of 0.367 mV Pa^{-1}. The 2D trampoline inspired mechanics design allows the TENG based E-skin exhibiting excellent stretchability that enable stable tactile sensing with unchanged signal outputs under strain up to ~ 40%. Else, a crosstalk shielding layer could effectively suppress the crosstalk among the TENG array [48]. Here, we employed transparent silver nanowires (AgNWs) networks as a shielding layer via directly spray-coating, which obviously reduces the electrical crosstalk in TENG based tactile sensor arrays. As a result, the tactile sensor array is capable of integration on various kind of curved surfaces including skin to distinguish the shapes of contact objects as well as high-resolution tactile mapping.

2. Experimental section

2.1. Mechanics modeling of electrode

The finite element analysis (FEA) commercial software ABAQUS (Analysis User's Manual 2016) was utilized to optimize the electrode layout and to study the corresponding mechanical characteristics. The objective was to decrease the strain level in copper layer under different typical loads. The Polydimethylsiloxane (PDMS) was modeled by hexahedron elements (C3D8R), the thin Copper foil (Cu, 200 nm thick) and polyimide (PI, 2 μm thick) layers were modeled by shell elements (S4R). The minimal element size was 1/8th of the width of the copper wires (10 μm), which ensured the convergence and the accuracy of the simulation results. The elastic modulus (E) and Poisson's ratio (ν) used in the analysis were $E_{Cu} = 115$ GPa and $\nu_{Cu} = 0.4$ for Cu; $E_{PI} = 2.5$ GPa and $\nu_{PI} = 0.34$ for PI; $E_{PDMS\_1} = 1$ MPa and $\nu_{PDMS\_1} = 0.5$ for top PDMS; $E_{PDMS\_2} = 70$ kPa and $\nu_{PDMS\_2} = 0.5$ for bottom PDMS.

2.2. Fabrication of the conductive layer

As shown in Fig. 1a, the conductive layer is based on copper electrode with trampoline inspired design. The fabrication process is shown in Fig. S1. The fabrication started on a pre-cleaned glass substrate, 20 mg/ml Poly(methylmethacrylate) (PMMA) solution was first spin-coated at 2000 rpm for 60 s on the glass, then cured on a hotplate at 200 °C for 20 min, serving as the sacrificial layer. Poly-amic acid solution (12.0 wt% ± 0.5 wt%) was spin-coated onto the PMMA layer at 3000 rpm for 30 s and then baked on a hotplate at 250 °C for 30 min to form a 2 μm thick PI film. Afterward, a 200 nm copper film was sputtered onto the PI layer, followed by spin-coating a 2 μm PI layer onto it that used the same procedure of the previous PI layer. The trampoline pattern of the electrode was formed through photolithography method: A layer of AZ4620 photoresist (PR, AZ 4620, AZ Electronic Materials) was spin-coated at 3000 rpm for 30 s on the surface of the top PI layer, then soft baked on a hotplate at 115 °C for 5 min, exposed to ultraviolet

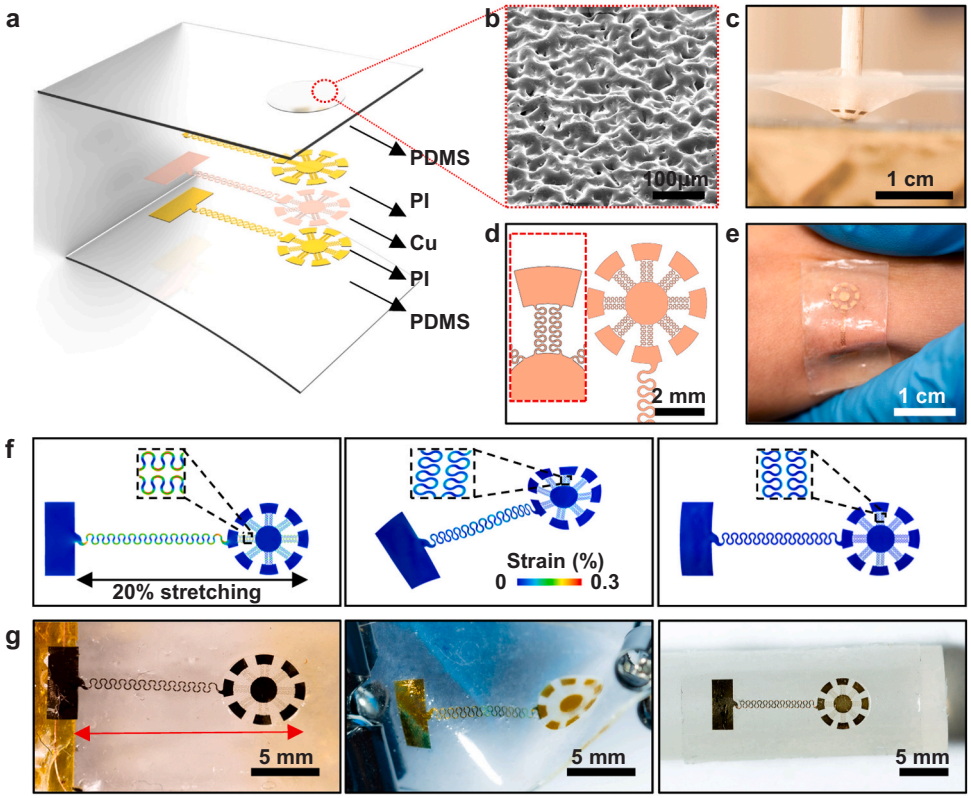

Fig. 1. Overview of the micro-structured and stretchable triboelectric nanogenerator. a) Schematic illustration of the triboelectric nanogenerator. b) The micro-structured surface of the PDMS triboelectric region. c) Under vertical poking, the TENG deforms like a trampoline. d) The sketch of the electrode layout and its enlarged view. e) Optical images of the TENG attached to human skin and deformed with skin. f), g) The FEA results of strain distributions and corresponding optical images of the TENG under stretching, twisting, and bending.

light for 45 s with a mask aligner (URE-2000/35AL deep UV, IOE, CAS), developed in AZ 400 K developer, followed by post-bake at 115 °C for 5 min, then the desired pattern was formed. Then, the top PI layer was selectively etched through reactive ion etching (RIE, Oxford Plasma-Therm 790 RIE system, 200 W, 10 min). Wet etching the exposed Cu thin film in Cu etchant and then rinsed by deionized water (DI water) and dry air below dried, followed by another process of dry etching of the bottom PI layer again. The remained PR layer was removed by acetone, and finally the desired electrode pattern with sandwich structure (PI/Cu/PI) was realized. Then, the PI on the rectangle part of the electrode pattern (Fig. 1a) was selectively etched by RIE again, exposing the copper layer for subsequent connection with copper wire. Immersed the electrode pattern into acetone for 12 h until the PMMA layer was completely dissolved. Next, a water-soluble tape (WST) acting as a stamp was attached on to the pattern tightly and picked electrode up. A PDMS (Sylgard 184, Dow Corning Corporation) substrate (spin-coating speed: 600 rpm, 30 s) and the electrode-attached WST were exposed to UV induced ozone together for 10 min, to create chemical groups for bonding between the bottom PI layer of electrode and PDMS substrate. Transfer printed the electrode through tightly attaching the WST to the PDMS substrate, followed by heating them in an oven at 90 °C for 10 min to further enhancing the bonding strength. Then immersed the WST-attached PDMS into water to remove the WST, leaving the electrode integrated onto the PDMS substrate tightly, they served as conductive layer and substrate respectively. Finally, connected the exposed copper part with copper wire by silver paste, for the following electrical performance test.

2.3. Fabrication of the triboelectric layer

Considering low-cost and ease-fabrication, we employed sandpapers as molds for microstructure duplicating. The schematic illustrations in Fig. S2 present a process of forming a PDMS top layer with a microstructured region serving as negative triboelectric layer. First, a piece

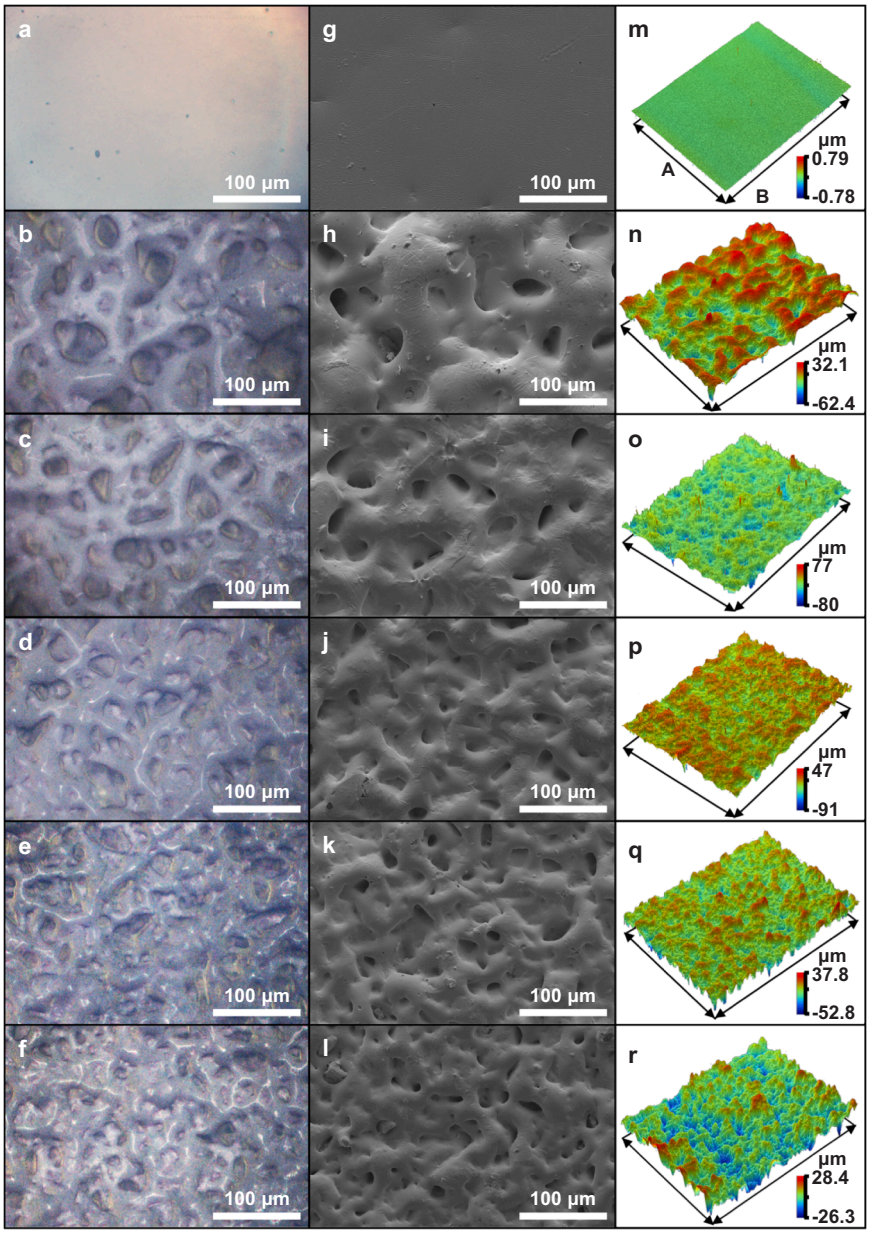

Fig. 2. The surface morphologies of PDMS with/without microstructure. a)–f) the optical images, g)–l) SEM images and m)–r) topographies of the plain PDMS surface, and those patterned with sandpapers of 400, 600, 800, 1000, 1200 respectively. (The topographies of corresponding samples were measured by the optical surface profiler (A: 671.0 μm, B: 896.4 μm)).

of sandpaper was pre-cleaned with acetone, ethanol, and DI water in sequence, and then fixed onto the surface of a glass sheet. Then a photolithography process was carried out as mentioned before, the difference is: the PR layer was formed through spin-coating (800 rpm, 30 s) for twice to completely cover the surface of the sandpaper, and the UV exposure time is 4 min followed by developing. Then the mold for microstructure patterns was obtained. Next, PDMS was prepared and placed in vacuum environment for 30 min to remove air bubbles. Spin-coating the PDMS onto the microstructure mold at 600 rpm for 30 s, then placed them in vacuum environment to sock the bubbles again. Transferred the PDMS coated sandpaper into an oven and cured at 70 °C for 1 h, the micro-structured pattern was formed below the PDMS layer. Since the PDMS has weak adhesion with PR and SiC particles of the sandpaper, the micro-structured PDMS layer could be easily peeled off from the mold. The PDMS top layer with a micro-structured region (5 mm in diameter) was realized. The improvement of the triboelectric effect would be affected by the morphology of surface. To analyze the relationship between the electrical performance of the TENG and morphology of the triboelectric layer, the sandpapers with grit size of 400, 600, 800, 1000, 1200 were utilized for the fabrication of micro-structure molds, while the plain triboelectric layer was also fabricated through spin-coating PDMS onto a glass sheet, at 600 rpm for 30 s.

2.4. Integration and assembly of the TENG

As shown in Fig. S2(g), after treated by O_2 plasma for 3 min, the back side of the triboelectric layer and the electrode-attached substrate were attached firmly together (the position of the micro-structured region was vertically corresponding to electrode pattern), finally the self-powered tactile sensor was assembled. The 4 × 4 sensor array was also fabricated through the same method. Additionally, silver nanowires (AgNWs) were utilized as crosstalk shielding material due to their great conductivity, transmittance and flexibility. The top layer of array was treated with O_2 plasma for 3 min, then a layer of AgNWs network was formed onto the top layer by spray-coating via a shadow mask. The AgNW layer was connected to the ground, serving as a shielding layer. All the units of the array were bond to anisotropic conductive films (ACFs) for datacollection and acquisition.

2.5. Characterizations

The surface morphologies of the PDMS triboelectric layers were characterized by field emission scanning electron microscopy (SEM, FEI Quanta 450 FEG SEM). The surface roughness was measured by the optical surface profiler (OSP, Veeco/Wyko NT9300). The force applied on the TENG was measured by a load cell (CHLBS-min, ChuDa sensors). The open-circuit voltage of the TENGs was measured by a DAQ multimeter (Keithley 6510, sampling rate: 60 kHz) with ultra-high resistance. The short-circuit current of the TENGs was calculated by measuring the voltage through the PowerLab data acquisition (PL3516/P Powerlab 16/35, AD Instruments, sampling rate: 10 kHz) with low noise of a fixed value resistor connecting in series with the TENG. The OC voltage of 4 × 4 array was also measured by the PowerLab data acquisition with its 16 analog input channels. The sheet resistance of silver nanowires networks was measured by a four-wire measurement (HPS2523). The TENG was operated and tested on a volunteer body with his full and informed consent.

3. Results and discussion

The schematic illustration of the stretchable TENG based single unit sensor cell is shown in Fig. 1a. The device adopts a single electrode mode for triboelectric electricity generation, where a thin soft PDMS layer (170 μm thick, E_{moduli} ~ 500 kPa) serves as the substrate, a photolithography-defined copper thin layer (Cu; 200 nm) supported and selectively encapsulated with two polyimide thin layers (PI; 2 μm) serves as electrode, and another PDMS layer (170 μm; E_{moduli} ~ 1 MPa) on top of the electrode encapsulates the device. The top PDMS encapsulation layer also serves as a functional triboelectric layer where the overlapped area (5 mm in diameter) with electrodes exhibits micro-

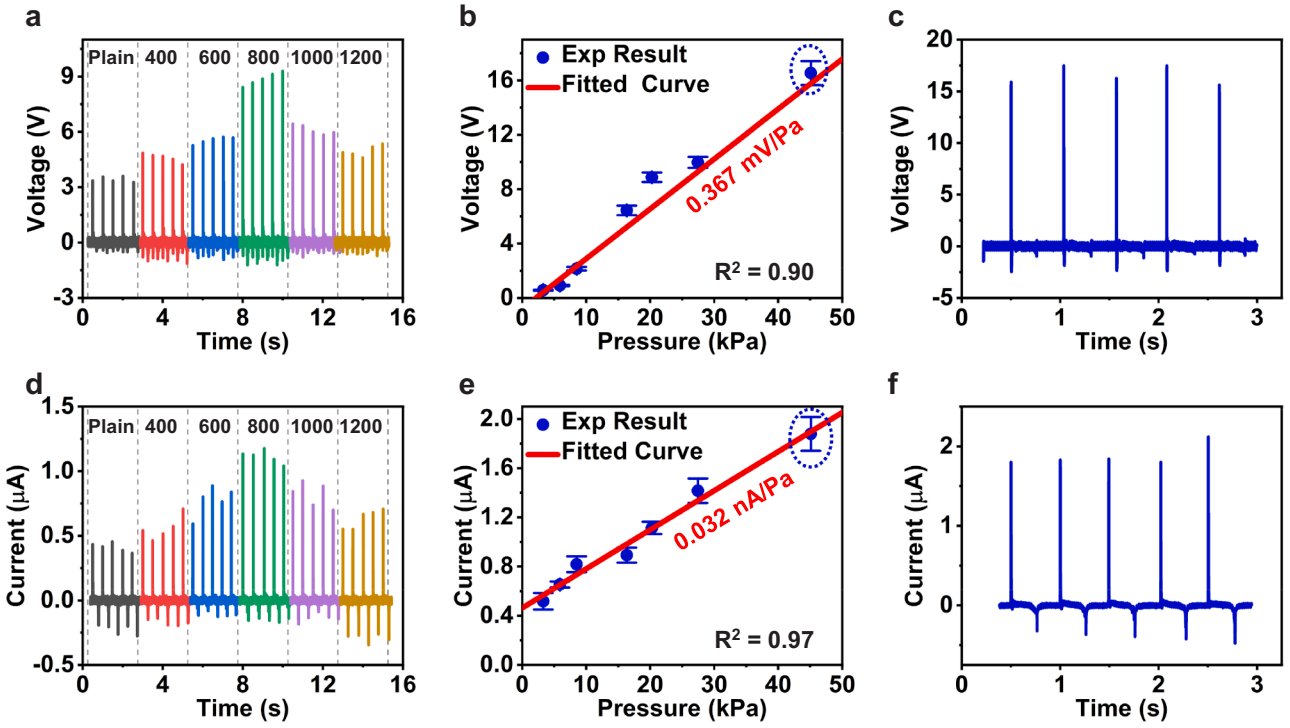

Fig. 3. The electrical characteristics of the TENG. a), d) The open-circuit voltage (OC voltage) and short-circuit current (SC current) of the TENG as a function of grit size in sandpapers, under constant stress of 20.26 kPa at frequency of 2 Hz. b), e) The OC voltage and SC current of TENG as a function of pressure at frequency of 2 Hz. c), f) The time dependent plots of OC voltage and the corresponding SC current under a pressure of ~ 45.1 kPa.

structures for enhancing the contact areas to induce more triboelectric charges. Sandpapers with different grit sizes were used as molds to create these micro-structures by directly casting PDMS on it, and the micro-structured region like frosted surfaces with various kinds of morphologies can be realized. The micro-structured PDMS thin layer exhibits considerable flexibility & stretchability, great negative-electron affinity and more effective contact areas for inducing charges, while the bottom PDMS layer serving as the substrate with lower modulus allows excellent adhesion with human skin by Van Der Waals forces. Fig. 1b shows the scanning electron microscope (SEM) image of a representative micro-structured feature in PDMS patterned by sandpapers, where micro-sized pyramid like structures can be observed in this region that would provide more contact area for triboelectric effect than that of a plain surface. The electrode adopts "trampoline" styled design, where a disc in the middle (1.8 mm in diameter) and with the whole region overlapped with the micro-structured region serves as conductive layer for triboelectric induced the charges, while 16 long serpentine metallic traces (width of 100 μm) in a symmetric arrangement act as "side springs" of the trampoline and connect with the small Cu thin film island. The trampoline inspired design offers great stretchability in both in-plane and out-of-plane directions. Fig. 1d shows the CAD design and the corresponding enlarged view of serpentine lines and islands. During a mechanical load induced triboelectric generation process, these islands are in charge of the majority part of the electrostatic charges induction, while the serpentine traces function as stretchable springs to link all the islands into an entirety. Fig. 1c displays the great mechanical advantage out of plane in the trampoline like device, where significant deformation in vertical direction wouldn't cause damage on the device. The thickness of the TENG device is 350 μm and weighs only 0.08 g/cm^2, which is thin and light enough to be conformally integrated with skin by its own adhesion force without additional tapes or straps. Evidences shown in Fig. 1e proves the prefect skin-integration behaviors of the device, that can be deformed with skin together under twisting, bending and stretching. The Fig. 1f, g shows the stimulated strain distributions of the copper layer under three type of typical deformations, and the corresponding optical images respectively, including 20% stretching, 70° twisting and bending with a radius of 5 mm. The finite element analysis (FEA) results indicate that under the deformations, the stimulated strains are significantly less than the copper yield strain 0.3%, which attribute to the sandwich structure of PI/Cu/PI, where the copper layer is placed at the mechanical neutral plane of the serpentine wires to minimize the strain/stress in copper layer due to bending. These testing results reveals the robust yet stretchable device can easily operate under realistic physiological loads. Corresponding to the FEA results, the optical image shows that under the deformations, the electrode maintained robust structure and without any cracks. The above results indicate that the design of islands-bridge layout successfully minimizes the strain level of copper electrode under various deformations, which endow the TENG electrode with the ability to integrate with the human body under daily motions.

Morphologies and microstructures of triboelectric layers in TENGs is a key issue for electrical performance as which can result in different contact electrification effects. The microstructures in the PDMS triboelectric layers in this work were created by sandpapers, so we employed and studied various sandpapers with different grit sizes, ranging from 400 to 1200 on the microstructures and electrical performance difference in PDMS triboelectric layers. As a reference, plain PDMS without any microstructure modifications was also studied as a bench mark. Figs. 2 and S3 show the optical, SEM images and the corresponding surface profiler characterized morphologies of the micro-structured PDMS layers by different sandpapers. The plain PDMS thin layer casted by spin-coating is quite smooth with an average root mean square (rms, R_{rms}) of 28.12 nm. Toward the patterned group, the particle-distributed microstructures were perfectly duplicated from sandpapers to PDMS surfaces. With the grit size increasing, the microstructures on PDMS surface become smaller and denser, resulting in roughness decrease, specifically, R_{rms} = 11.98 μm for grit size-400 to R_{rms} = 7.14 μm for grit size-1200 (Table S1).

Next, the relationship between the electrical performance of TENG devices and the microstructures formed from different grit sized sandpapers was studied to clarify the most optimized parameters. The tests of TENG devices associated with contact-separation between the triboelectric region and a contact object with contact area of 8 × 8 mm^2. Since the contact area during the test is much larger than that of the working region (5 mm in diameter) in the TENG devices, the measurement can guarantee stable and reliable data. For the purpose of developing self-powered tactile sensors, fingers and some daily used objects are the most relevant contact objects that couple with the triboelectric

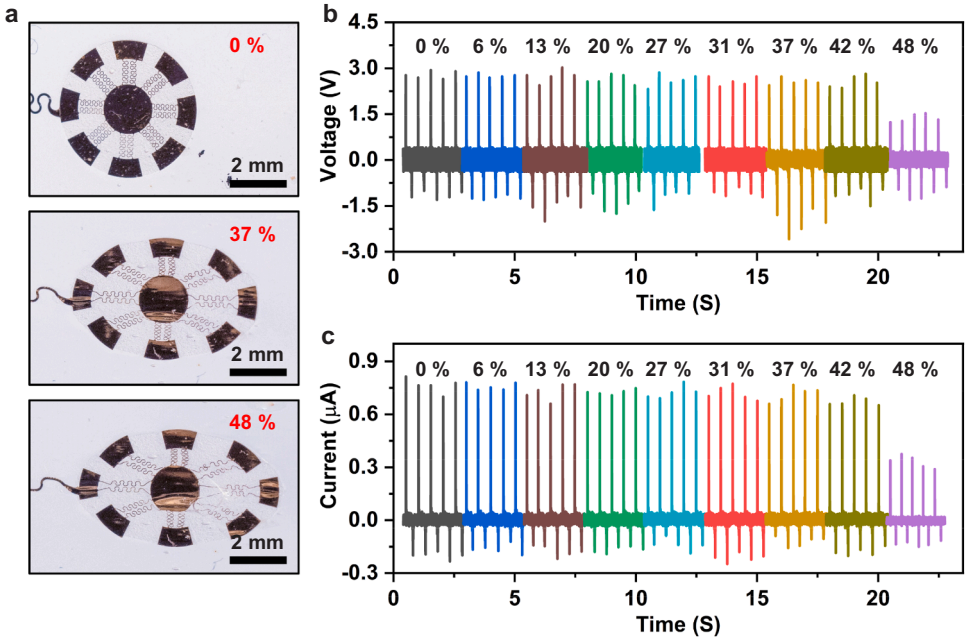

Fig. 4. Stretchability test of the TENG. a) Optical images of the TENG under 0%, 37%, and 48% strain. b), c) the OC voltage and corresponding SC current of the TENG as function of various strain levels from 0% to 48%, under constant stress of 9.42 kPa at frequency of 2 Hz.

region in TENGs. The open-circuit (OC) voltage and short-circuit (SC) current were systemically characterized via a self-built mechanical loading machine. Fig. S4 shows the working principle of the TENG devices, where skin and the micro-structured PDMS region serve as positive and negative triboelectric layers, respectively. When a finger touched the triboelectric region, the skin partially deformed and morphologically approaching with the uneven surface of the triboelectric region, result in larger contact area for more charges generation than that of contacting with a plain PDMS surface. Under a periodical pressure of ~ 20 kPa at a frequency of 2 Hz, the OC voltage (Fig. 3a) and SC current (Fig. 3d) in TENGs as a function of grit sizes present an interesting variation trend. First, all the microstructures patterned devices exhibit greater electrical signal outputs than that of the plain group. The OC voltage and SC current are only 3.43 ± 0.14 V and 0.41 ± 0.04 μA for the plain PDMS based devices, while the patterned group shows OC voltage and SC current of 4.60 ± 0.24 V and 0.56 ± 0.10 μA for devices with grit sizes of 400, 8.88 ± 0.35 V and 1.11 ± 0.05 μA for devices with grit sizes of 800. However, further increasing the grit sizes causes outputs deterioration, with 6.12 ± 0.25 V and 0.82 ± 0.09 μA for grit sizes of 1000, and 4.97 ± 0.29 V and 0.63 ± 0.08 μA for grit sizes of 1200. Lower grit sizes enhancing performance can be easily understood as the increase of effective triboelectric contact area, however, higher grit sizes caused performance deterioration is because the concave holes/cavities are too small to provide effective areas. It is clear that the microstructures produced by sandpaper of 800 grit size offer the best magnification of contact electrification effect, so devices patterned by 800 grit size was selected for more detail tests and demonstrations.

Fig. 3b, e shows the OC voltage and SC current of the 800 grit sized sandpapers modified TENG devices as a function of various applied stress, ranging from ~ 3 kPa to ~ 45 kPa at a fixed frequency of 2 Hz, which is within the typical range for tactile sensor and E-skin [45,49,50]. The resulting outputs were measured to be 574.66 ± 0.03 mV and 0.52 ± 0.07 μA and 16.55 ± 0.88 V and 1.88 ± 0.14 μA, at a very gentle touching force of 3.27 kPa and a more solid touching force of 45.1 kPa, indicating the great capability for sensing various types of touching with different stress. The TENG device also presents a great linearity with applied stress for both the OC voltage and SC current outputs, with a sensitivity of 0.367 mV Pa^{-1}. Due to the small induced area, the sensitivity of the sensors is not the greatest compared to previous reported TENG based ones (Table S2) [43,46,51–54]. However, the flexibility and stretchability of our devices can offer more applications scenarios. Representative plots of signal outputs in the TENG vs time are shown in Fig. 3c, f, revealing repeatable and stable time dependent waveforms, demonstrating considerable and constantly stable output amplitudes. In

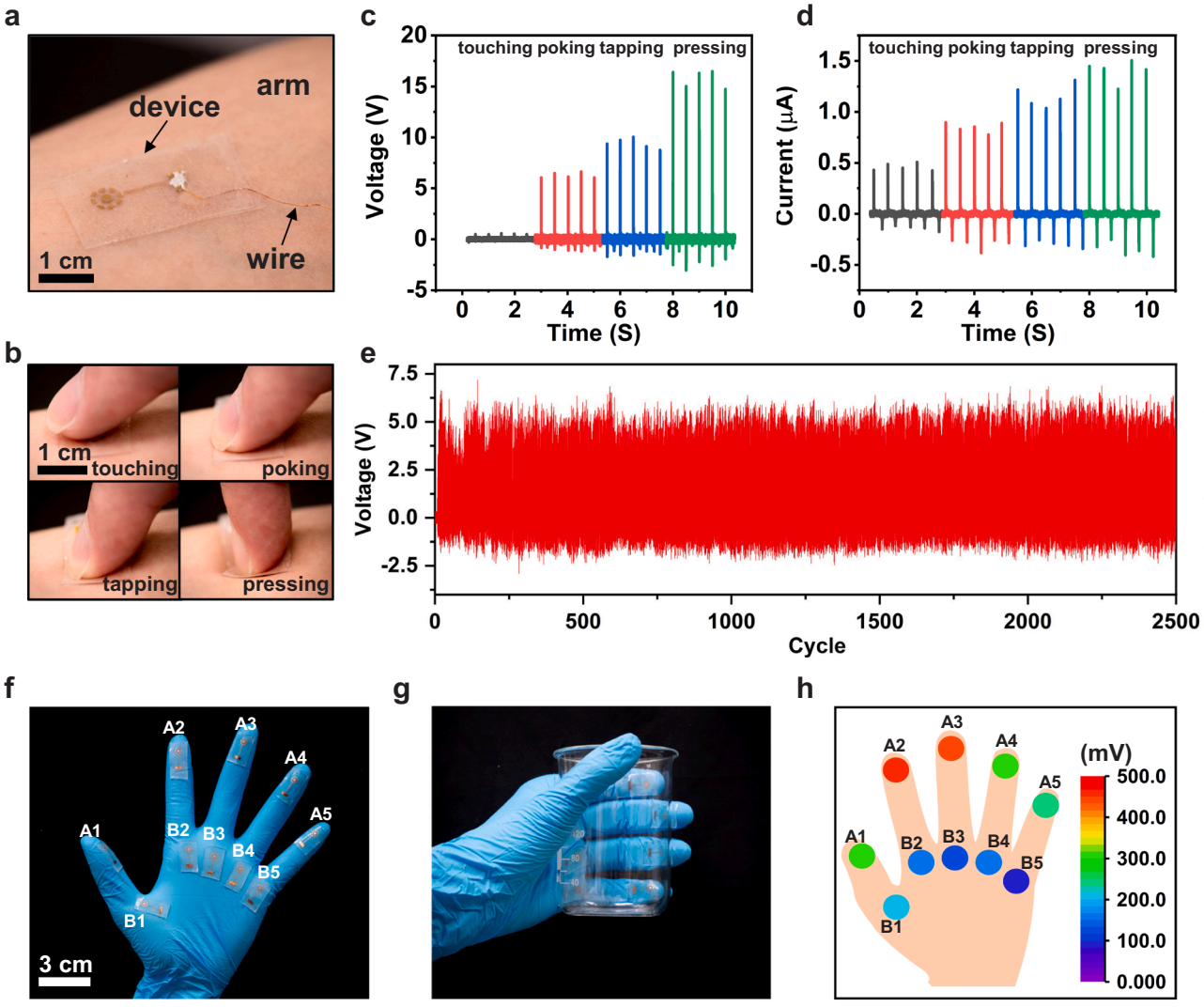

Fig. 5. The TENG for skin-integrated tactile sensing. a) Optical images of the TENG mounted on human skin, and b) touched, poked, tapped and press by human finger. c), d) The corresponding OC voltage and SC current of the TENG under different loads by a finger. e) The OC voltage of the TENG, under a constant taping by finger (15–23 kPa), at frequency 4 Hz for 2500 cycles. f) the optical image of a glove with 10 TENGs integrated on different locations and g) the moment when TENGs-integrated glove holding a 200 ml beaker. h) The distributions of OC voltage while holding the beaker.

view of the above excellent electrical performance, the TENG devices are capable of tactile sensing for activities in human's in daily life.

Normal daily activities related strain levels of human skin could be up to 20–30%, thereby the skin-integrated sensors that can undertake the corresponding strains are of great significance. Here axial and dual-directional stretchability test of the TENG based sensors were carried out by a self-built stretching stage. The strain level is defined as the ratio of changing length to the original length of the electrode. The device shows similar deformation feature under strain levels from 0% to 48% in either x axial or y axial strain, since the device adopts a symmetrical design (Fig. S5). The Figs. 4a and S6 show the photos and the microscope captured images of a representative TENG sensor under y axial strains of 0%, 37% and 48%, where the deformations presented here are in great agreement with strain distributions stimulated by FEA (Fig. 1f). Some visible fracture failures may occur in the interconnects between islands and serpentine bridges under strain above 42%, but each small island was still linked to the central one via unbroken traces, thus the effective induced-area is almost unchanged (Figs. S5d, e and S7). The Fig. 4b shows the OC voltage and SC current of the TENG as a function of various strain levels ranging from 0% to 48%, under a constant pressure of ~ 9 kPa at frequency of 2 Hz. It can be seen that the TENG sensor can maintain almost unchanged electrical outputs up to 42% stretching, due to the similar induced-area, while the output signals deteriorated under further stretching to 48%, due to the broken of the serpentine traces. Therefore, we concluded that the 42% stretching is the ultimate strain for operation of our device, which is comparable or even greater than that of devices with intrinsically stretchable conductors (Table. S2). Furtherly, we also tested the performance of the sole center island in the

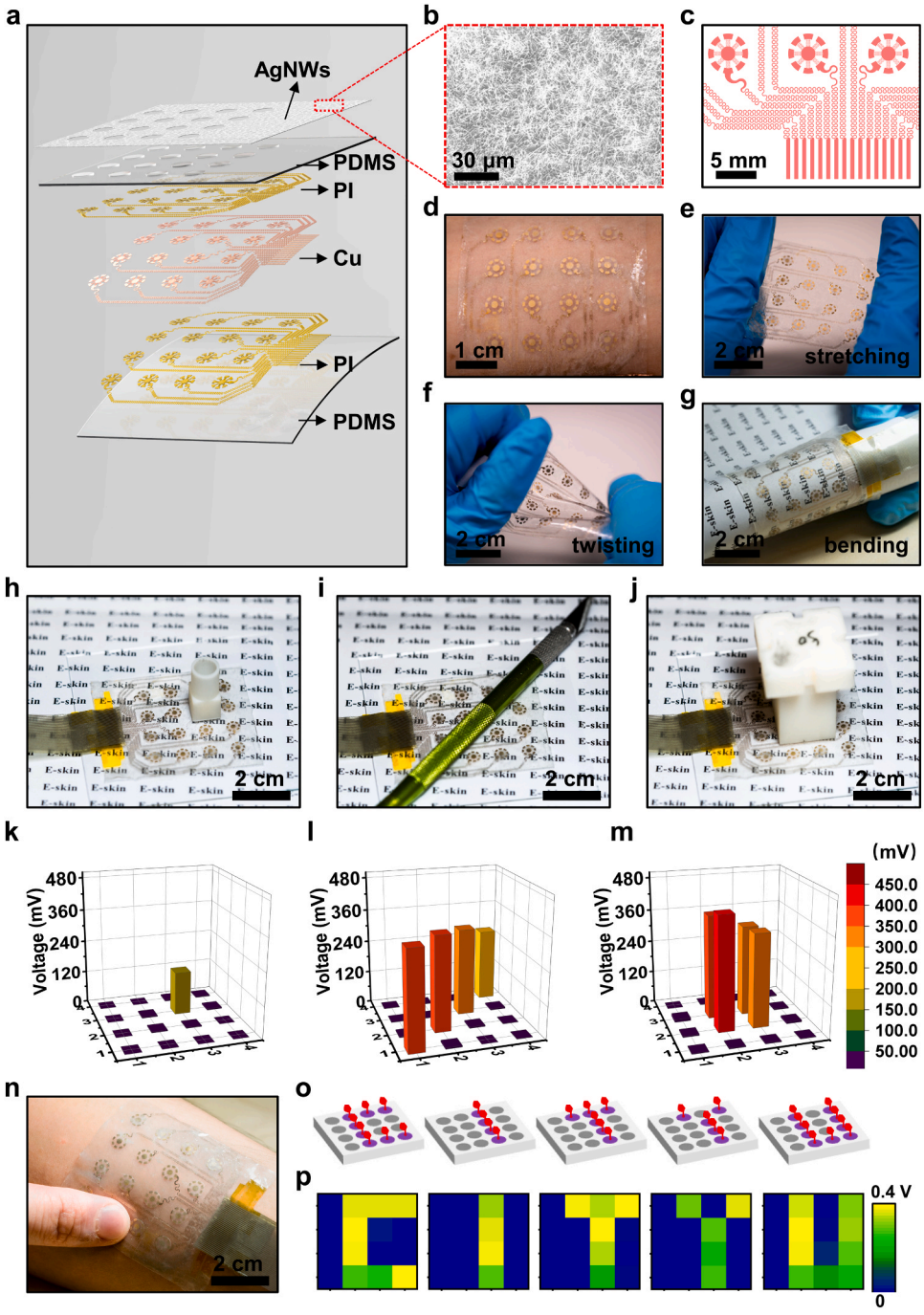

Fig. 6. The 4 × 4 tactile sensor array E-skin a) Schematic illustration of the 4 × 4 sensor array. b) the SEM image of the AgNWs layer (the average sheet resistance of the AgNWs layer: 42.0 Ω/sq). c) The enlarged illustration of the array layout. d) The optical images of the array mounted on human arm. e)–g) The array under mechanical deformations including stretching, twisting and bending respectively. h)–j) The optical images and k)–m) corresponding OC Voltage distribution of the sensor array mapping for by different objects, including a small resin block (1.64 g), a knife cutter (15.87 g) and a big resin block (24.63 g) respectively. (n) The TENG array serving as E-skin mounted on arm and touched by finger with a pattern of "CITYU". (o), (p) The schematic illustration of the sensor array touched by finger with a pattern of "CITYU" and the corresponding OC voltage distribution.

device (Fig. S8a–d) by using a bamboo stick, the results shown in Fig. S8e indicate that the islands could perform electrostatic induction independent of trace straightening until all the traces fracture. Similarity, the TENG could perform durable output and maintain great robust structure even under dual-directional stretching of ~ 20% (Figs. S9 and S10), with a hard vertical poking to the depth up to 7 mm (Fig. S11). These comprehensive experiments show the excellent stretchability of the trampoline inspired TENGs for 3 dimensional deformations, that can eliminate the undesired influence and coupling issues induced by either in-plane or out-plane stretching.

In order to evaluate the practical application of the TENG sensors in realistic scenarios, one TENG single cell sensor was integrated on a volunteer's arm serving as E-skin for tactile sensing (Fig. 5a). Four types of common force by an index finger referring touching (3.01 ± 0.78 kPa), poking (15.43 ± 1.12 kPa), tapping (26.31 ± 1.45 kPa) and pressing (44.62 ± 3.11 kPa) were introduced to test the corresponding OC voltage and SC current. As shown in Fig. 5b, different types of forces causing significant difference of skin deformation, meanwhile the TENG sensor can be conformably integrated with skin without delamination in all situations. The outputs of OC voltage and SC current in the TENG under four types of loads were presented in Fig. 5c, d, with 0.50 ± 0.03 V and 0.46 ± 0.04 μA for touching, 6.27 ± 0.27 V and 0.85 ± 0.05 μA for poking, 9.41 ± 0.51 V and 1.16 ± 0.11 μA for tapping, and 15.79 ± 0.84 V and 1.41 ± 0.11 μA for pressing, respectively. To study the durability of the TENG sensor in realistic applications, we characterized a reprehensive sensor by a finger poking (11.3–16.4 kPa) at frequency of 2 Hz for over 2500 cycles, where the signal outputs of the TENG was very stable (Fig. 5e). No cracks and fractures of the electrodes in the TENG devices were observed by the microscope, even after thousands of cycles of testing, that explained the robust performance of the devices (Fig. S12). Furthermore, the TENG device also maintained good adhesion with skin without any evidence of delamination, showing its durability and great potential in long-term skin-integration (Fig. S13 and Movie S1). Encouraged by the excellent electrical and mechanical properties of the E-skin TENG sensors, a smart glove assembling with 10 sensors at finger and palm areas were developed to show the potential application in human-machine interfacing and tactile mapping. Due to the low modulus of the substrate used in the TENGs, the devices can be directly mounted on the latex glove through Van Der Waals forces without additional tapes, and thus these sensors can act as tactile sensing units for mapping tactile information when grabbing an object (Fig. 5f, g). The smart glove can detect synchronous signals from different sensing unit (Fig. S14), and thus mapping the gesture and force distribution when holding a baker (Fig. 5h).

Supplementary material related to this article can be found online at doi:10.1016/j.nanoen.2020.105590.

Next, the 16 TENG sensors were assembled together to form a 4×4 self-powered E-skin tactile-sensing array for multiple-points tactile sensing. As shown in Fig. 6a, every TENG sensor serves as one tactile sensing unit cell, spacing 5 mm away from each other, and serpentine metallic traces connecting each unit individually for data collection and acquisition by an anisotropic conductive film (Fig. 6c). A layer of AgNWs networks (average sheet resistance of 42 Ω/sq) covers the top layer of the array except for the micro-structured regions, serves as the shielding layer (Fig. 6b). The overall dimension of the arrayed device is 63 mm × 47 mm × 350 μm, and the weight is only 120 mg. Like the single sensor unit, the soft nature of the sensor array allows it being capable to mount on skin tightly through Van Der Waals force (Fig. 6d). The sensor array is also very robust that can be survived even after a series of intense deformations including stretching, twisting and bending (Fig. 6e–g), with unchanged performance. To evaluate the capabilities of pressure mapping, three objects, including a small plastic block (1.64 g), a cutter (15.87 g) and a big plastic block (24.63 g) were sequentially put on the array and the sensing signal outputs were collected (Fig. 6h–j). The sensing signals were accurately detected that can reveal information from the positions, to the weight of the tested objects (Fig. 6k–m). The signal output amplitudes generally reflect the weights of the tested objects, however crosstalk is a very challenge problem in TENG based sensing arrays when the output is not great enough. Here, the TENG based array introduced AgNWs networks as the shielding layer that significantly solved the crosstalk issue, where the signals induced from no-contacted sensors were far lower (< 25 mV) than the signal detected by the contact sensors (> hundreds mV). The great improvement owes to the AgNWs networks on non-sensing areas which significantly eliminate the electrostatic charges induction between neighbor sensing units. As a result, the signal distributions reveal great reflections of the objects' weights and shapes. In addition to demonstrate the sensor array on a rigid platform, we also integrated the device with skin (Fig. 6n), where a volunteer wearing the E-skin sensor array on his forearm, and wrote letters "CITYU" by a finger on the E-skin (Fig. 6o). As a result, the corresponding signals in the sensor array distributed as the same written pattern, with a maximum peak voltage of 400 mV and crosstalk free (Fig. 6p and Movie S2). Furthermore, the AgNWs networks is completely transparent and intrinsically stretchable that offers a new route for shielding technologies, while the spray-coated AgNWs film still could not guarantee reliable conductivity when acts as electrode with micron width, due to the local sparse and dense distribution. However, the one point - one channel style sensing array occupies more spaces and limits the resolution. In fact, some novel strategies for single-electrode mode array and crosstalk suppression have been developed [55], indicating a bright future in TENG-based E-skin. Overall, the E-skin array exhibit excellent performance for multiple-points tactile sensing with high accuracy and large scale, which is quite practical in wearable applications like artificial skin and flexible keyboards.

Supplementary material related to this article can be found online at doi:10.1016/j.nanoen.2020.105590.

4. Conclusion

In summary, thin, soft, stretchable, skin-integrated and self-powered E-skin tactile sensors based on triboelectric effect were reported. The trampoline inspired mechanics design afforded the E-skin TENG sensors excellent stretchability, stable electrical performance and great long-term durability. The simple sandpaper severed as mold enabled realizing microstructures in the triboelectric layer that can significantly improve the electrical performance of the soft TENGs. Furthermore, simple coating AgNWs networks allowed the TENGs to be integrated into sensing arrays with no crosstalk issue. The reported TENG E-skin has been proved the potential in tactile sensing, pressure mapping and human-machine interface, indicating its brilliant prospect in more self-power wearable applications.

CRediT authorship contribution statement

Jiahui He: Investigation, Formal analysis, Data curation, Writing - original draft. **Zhaoqian Xie**: Formal analysis, Conceptualization, Visualization, Funding acquisition. **Kuanming Yao**: Investigation, Validation. **Dengfeng Li:** Investigation, Methodology. **Yiming Liu**: Investigation. **Zhan Gao**: Investigation. **Wei Lu**: Investigation. **Lingqian Chang**: Investigation. **Xinge Yu**: Writing - review & editing, Supervision, Project administration, Funding acquisition.

Declaration of Competing Interest

The authors declare that they have no known competing financial interests or personal relationships that could have appeared to influence the work reported in this paper.

Acknowledgments

J.H. and Z.X. contributed equally to this work. This work was

supported by City University of Hong Kong (Grants Nos. 9610423, 9667199), Research Grants Council of Hong Kong Special Administrative Region (Grant No. 21210820), Shenzhen Science and Technology Innovation Commission (Grant No. JCYJ20200109110201713), Department of Science and Technology of Sichuan Province (Grant No. 2020YFH0181), National Natural Science Foundation of China (Grant No. 12072057), and Fundamental Research Funds for the Central Universities (Grant No. DUT20RC(3)032).

Appendix A. Supplementary material

Supplementary data associated with this article can be found in the online version at doi:10.1016/j.nanoen.2020.105590.

References

[1] H. Wu, W. Gao, Z. Yin, Materials, devices and systems of soft bioelectronics for precision therapy, Adv. Healthc. Mater. 6 (2017), 1700017.
[2] H. Lee, C. Song, S. Baik, D. Kim, T. Hyeon, D.H. Kim, Device-assisted transdermal drug delivery, Adv. Drug Deliv. Rev. 127 (2018) 35–45.
[3] S. Choi, H. Lee, R. Ghaffari, T. Hyeon, D.-H. Kim, Recent advances in flexible and stretchable bio-electronic devices integrated with nanomaterials, Adv. Mater. 28 (2016) 4203–4218.
[4] Y. Khan, A.E. Ostfeld, C.M. Lochner, A. Pierre, A.C. Arias, Monitoring of vital signs with flexible and wearable medical devices, Adv. Mater. 28 (2016) 4373–4395.
[5] H.-R. Lim, H.S. Kim, R. Qazi, Y.-T. Kwon, J.-W. Jeong, W.-H. Yeo, Advanced soft materials, sensor integrations, and applications of wearable flexible hybrid electronics in healthcare, energy, and environment, Adv. Mater. 32 (2020), 1901924.
[6] H. Xu, J.X. Xiang, Y.F. Lu, M.K. Zhang, J.J. Li, B.B. Gao, Y.J. Zhao, Z.Z. Gu, Multifunctional wearable sensing devices based on functionalized graphene films for simultaneous monitoring of physiological signals and volatile organic compound biomarkers, ACS Appl. Mater. Interfaces 10 (2018) 11785–11793.
[7] X. Yu, Z. Xie, Y. Yu, J. Lee, A. Vazquez-Guardado, H. Luan, J. Ruban, X. Ning, A. Akhtar, D. Li, B. Ji, Y. Liu, R. Sun, J. Cao, Q. Huo, Y. Zhong, C. Lee, S. Kim, P. Gutruf, C. Zhang, Y. Xue, Q. Guo, A. Chempakasseril, P. Tian, W. Lu, J. Jeong, Y. Yu, J. Cornman, C. Tan, B. Kim, K. Lee, X. Feng, Y. Huang, J.A. Rogers, Skin-integrated wireless haptic interfaces for virtual and augmented reality, Nature 575 (2019) 473–479.
[8] J.C. Yang, J. Mun, S.Y. Kwon, S. Park, Z. Bao, S. Park, Electronic skin: recent progress and future prospects for skin-attachable devices for health monitoring, robotics, and prosthetics, Adv. Mater. 31 (2019), 1904765.
[9] K. Sim, Z. Rao, Z. Zou, F. Ershad, J. Lei, A. Thukral, J. Chen, Q.-A. Huang, J. Xiao, C. Yu, Metal oxide semiconductor nanomembrane–based soft unnoticeable multifunctional electronics for wearable human-machine interfaces, Sci. Adv. 5 (2019), eaav9653.
[10] S. Choi, S.I. Han, D. Jung, H.J. Hwang, C. Lim, S. Bae, O.K. Park, C.M. Tschabrunn, M. Lee, S.Y. Bae, J.W. Yu, J.H. Ryu, S.-W. Lee, K. Park, P.M. Kang, W.B. Lee, R. Nezafat, T. Hyeon, D.-H. Kim, Highly conductive, stretchable and biocompatible Ag–Au core–sheath nanowire composite for wearable and implantable bioelectronics, Nat. Nanotechnol. 13 (2018) 1048–1056.
[11] M. Wang, P. Baek, A. Akbarinejad, D. Barker, J. Travas-Sejdic, Conjugated polymers and composites for stretchable organic electronics, J. Mater. Chem. C 7 (2019) 5534–5552.
[12] A.J. Bandodkar, R. Nuñez-Flores, W. Jia, J. Wang, All-printed stretchable electrochemical devices, Adv. Mater. 27 (2015) 3060–3065.
[13] Y. Kim, J. Zhu, B. Yeom, M. Di Prima, X. Su, J.-G. Kim, S.J. Yoo, C. Uher, N. A. Kotov, Stretchable nanoparticle conductors with self-organized conductive pathways, Nature 500 (2013) 59–63.
[14] N. Matsuhisa, M. Kaltenbrunner, T. Yokota, H. Jinno, K. Kuribara, T. Sekitani, T. Someya, Printable elastic conductors with a high conductivity for electronic textile applications, Nat. Commun. 6 (2015) 7461.
[15] S. Zhang, Y. Li, Q. Tian, L. Liu, W. Yao, C. Chi, P. Zeng, N. Zhang, W. Wu, Highly conductive, flexible and stretchable conductors based on fractal silver nanostructures, J. Mater. Chem. C 6 (2018) 3999–4006.
[16] J. Park, S. Wang, M. Li, C. Ahn, J.K. Hyun, D.S. Kim, D.K. Kim, J.A. Rogers, Y. Huang, S. Jeon, Three-dimensional nanonetworks for giant stretchability in dielectrics and conductors, Nat. Commun. 3 (2012) 916.
[17] Q. Hua, J. Sun, H. Liu, R. Bao, R. Yu, J. Zhai, C. Pan, Z.L. Wang, Skin-inspired highly stretchable and conformable matrix networks for multifunctional sensing, Nat. Commun. 9 (2018) 244.
[18] S.-K. Kang, R.K.J. Murphy, S.-W. Hwang, S.M. Lee, D.V. Harburg, N.A. Krueger, J. Shin, P. Gamble, H. Cheng, S. Yu, Z. Liu, J.G. McCall, M. Stephen, H. Ying, J. Kim, G. Park, R.C. Webb, C.H. Lee, S. Chung, D.S. Wie, A.D. Gujar, B. Vemulapalli, A.H. Kim, K.-M. Lee, J. Cheng, Y. Huang, S.H. Lee, P.V. Braun, W. Z. Ray, J.A. Rogers, Bioresorbable silicon electronic sensors for the brain, Nature 530 (2016) 71–76.
[19] J. Yang, R. Shi, Z. Lou, R. Chai, K. Jiang, G. Shen, Flexible smart noncontact control systems with ultrasensitive humidity sensors, Small 15 (2019), 1902801.
[20] J. Hanna, M. Bteich, Y. Tawk, A.H. Ramadan, B. Dia, F.A. Asadallah, A. Eid, R. Kanj, J. Costantine, A.A. Eid, Noninvasive, wearable, and tunable electromagnetic multisensing system for continuous glucose monitoring, mimicking vasculature anatomy, Sci. Adv. 6 (2020), eaba5320.
[21] F.J. Romero, E. Castillo, A. Rivadeneyra, A. Toral-Lopez, M. Becherer, F.G. Ruiz, N. Rodriguez, D.P. Morales, Inexpensive and flexible nanographene-based electrodes for ubiquitous electrocardiogram monitoring, npj Flex. Electron. 3 (2019) 12.
[22] S. Lin, J. Liu, W. Li, D. Wang, Y. Huang, C. Jia, Z. Li, M. Murtaza, H. Wang, J. Song, Z. Liu, K. Huang, D. Zu, M. Lei, B. Hong, H. Wu, A flexible, robust, and gel-free electroencephalogram electrode for noninvasive brain-computer interfaces, Nano Lett. 19 (2019) 6853–6861.
[23] A. Chortos, J. Liu, Z. Bao, Pursuing prosthetic electronic skin, Nat. Mater. 15 (2016) 937–950.
[24] M.L. Hammock, A. Chortos, B.C. Tee, J.B. Tok, Z. Bao, 25th Anniversary article: the evolution of electronic skin (e-skin): a brief history, design considerations, and recent progress, Adv. Mater. 25 (2013) 5997–6038.
[25] J.C. Yang, J. Mun, S.Y. Kwon, S. Park, Z. Bao, S. Park, Electronic skin: recent progress and future prospects for skin-attachable devices for health monitoring, robotics, and prosthetics, Adv. Mater. 31 (2019), 1904765.
[26] F. Suarez, D.P. Parekh, C. Ladd, D. Vashaee, M.D. Dickey, M.C. Öztürk, Flexible thermoelectric generator using bulk legs and liquid metal interconnects for wearable electronics, Appl. Energy 202 (2017) 736–745.
[27] A. Nozariasbmarz, H. Collins, K. Dsouza, M.H. Polash, M. Hosseini, M. Hyland, J. Liu, A. Malhotra, F.M. Ortiz, F. Mohaddes, V.P. Ramesh, Y. Sargolzaeiaval, N. Snouwaert, M.C. Özturk, D. Vashaee, Review of wearable thermoelectric energy harvesting: from body temperature to electronic systems, Appl. Energy 258 (2020), 114069.
[28] Y. Liu, L. Zhao, L. Wang, H. Zheng, D. Li, R. Avila, K.W.C. Lai, Z. Wang, Z. Xie, Y. Zi, X. Yu, Skin-integrated graphene-embedded lead zirconate titanate rubber for energy harvesting and mechanical sensing, Adv. Mater. Technol. 4 (2019), 1900744.
[29] B.Z. Tian, X.L. Zheng, T.J. Kempa, Y. Fang, N.F. Yu, G.H. Yu, J.L. Huang, C. M. Lieber, Coaxial silicon nanowires as solar cells and nanoelectronic power sources, Nature 449 (2007) 885–U888..
[30] Q. Guo, J. Koo, Z. Xie, R. Avila, X. Yu, X. Ning, H. Zhang, X. Liang, S.B. Kim, Y. Yan, M.R. MacEwan, H.M. Lee, A. Song, Z. Di, Y. Huang, Y. Mei, J.A. Rogers, A bioresorbable magnetically coupled system for low-frequency wireless power transfer, Adv. Funct. Mater. 29 (2019), 1905451.
[31] L. Zhao, Q. Zheng, H. Ouyang, H. Li, L. Yan, B. Shi, Z. Li, A size-unlimited surface microstructure modification method for achieving high performance triboelectric nanogenerator, Nano Energy 28 (2016) 172–178.
[32] H. Yang, Y. Pang, T. Bu, W. Liu, J. Luo, D. Jiang, C. Zhang, Z.L. Wang, Triboelectric micromotors actuated by ultralow frequency mechanical stimuli, Nat. Commun. 10 (2019) 2309.
[33] C. Xu, B.B. Zhang, A.C. Wang, H.Y. Zou, G.L. Liu, W.B. Ding, C.S. Wu, M. Ma, P. Z. Peng, Z.Q. Lin, Z.L. Wang, Contact-electrification between two identical materials: curvature effect, ACS Nano 13 (2019) 2034–2041..
[34] F.-R. Fan, Z.-Q. Tian, Z. Lin Wang, Flexible triboelectric generator, Nano Energy 1 (2012) 328–334.
[35] F.-R. Fan, L. Lin, G. Zhu, W. Wu, R. Zhang, Z.L. Wang, Transparent triboelectric nanogenerators and self-powered pressure sensors based on micropatterned plastic films, Nano Lett. 12 (2012) 3109–3114.
[36] Z. Ren, J. Nie, J. Shao, Q. Lai, L. Wang, J. Chen, X. Chen, Z.L. Wang, Fully elastic and metal-free tactile sensors for detecting both normal and tangential forces based on triboelectric nanogenerators, Adv. Funct. Mater. 28 (2018), 1802989.
[37] D. Tantraviwat, P. Buarin, S. Suntalelat, W. Sripumkhai, P. Pattamang, G. Rujijanagul, B. Inceesungvorn, Highly dispersed porous polydimethylsiloxane for boosting power-generating performance of triboelectric nanogenerators, Nano Energy 67 (2020), 104214.
[38] X. Pu, H. Guo, Q. Tang, J. Chen, L. Feng, G. Liu, X. Wang, Y. Xi, C. Hu, Z.L. Wang, Rotation sensing and gesture control of a robot joint via triboelectric quantization sensor, Nano Energy 54 (2018) 453–460.
[39] F. Wen, Z. Sun, T. He, Q. Shi, M. Zhu, Z. Zhang, L. Li, T. Zhang, C. Lee, Machine learning glove using self-powered conductive superhydrophobic triboelectric textile for gesture recognition in VR/AR applications, Adv. Sci. 7 (2020), 2000261.
[40] C. Lu, J. Chen, T. Jiang, G. Gu, W. Tang, Z.L. Wang, A stretchable, flexible triboelectric nanogenerator for self-powered real-time motion monitoring, Adv. Mater. Technol. 3 (2018), 1800021.
[41] Z. Zhou, S. Padgett, Z. Cai, G. Conta, Y. Wu, Q. He, S. Zhang, C. Sun, J. Liu, E. Fan, K. Meng, Z. Lin, C. Uy, J. Yang, J. Chen, Single-layered ultra-soft washable smart textiles for all-around ballistocardiograph, respiration, and posture monitoring during sleep, Biosens. Bioelectron. 155 (2020), 112064.
[42] X.X. Zhu, X.S. Meng, S.Y. Kuang, X.D. Wang, C.F. Pan, G. Zhu, Z.L. Wang, Triboelectrification-enabled touch sensing for self-powered position mapping and dynamic tracking by a flexible and area-scalable sensor array, Nano Energy 41 (2017) 387–393.
[43] X. Pu, M. Liu, X. Chen, J. Sun, C. Du, Y. Zhang, J. Zhai, W. Hu, Z.L. Wang, Ultrastretchable, transparent triboelectric nanogenerator as electronic skin for biomechanical energy harvesting and tactile sensing, Sci. Adv. 3 (2017), e1700015.
[44] K. Yao, Y. Liu, D. Li, J. He, J. Li, R.H.W. Lam, Z. Xie, L. Wang, X. Yu, Mechanics designs-performance relationships in epidermal triboelectric nanogenerators, Nano Energy 76 (2020), 105017.
[45] Y. Liu, L. Wang, L. Zhao, K. Yao, Z. Xie, Y. Zi, X. Yu, Thin, skin-integrated, stretchable triboelectric nanogenerators for tactile sensing, Adv. Electron. Mater. 6 (2020), 1901174.

[46] H. Kang, C. Zhao, J. Huang, D.H. Ho, Y.T. Megra, J.W. Suk, J. Sun, Z.L. Wang, Q. Sun, J.H. Cho, Fingerprint-inspired conducting hierarchical wrinkles for energy-harvesting e-skin, Adv. Funct. Mater. 29 (2019), 1903580.
[47] X. Peng, K. Dong, C. Ye, Y. Jiang, S. Zhai, R. Cheng, D. Liu, X. Gao, J. Wang, Z. L. Wang, A breathable, biodegradable, antibacterial, and self-powered electronic skin based on all-nanofiber triboelectric nanogenerators, Sci. Adv. 6 (2020), eaba9624.
[48] X.X. Zhu, Z.B. Li, X.S. Li, L. Su, X.Y. Wei, S.Y. Kuang, B.W. Su, J. Yang, Z.L. Wang, G. Zhu, Triboelectrification-enabled thin-film tactile matrix for self-powered high-resolution imaging, Nano Energy 50 (2018) 497–503.
[49] J. Park, Y. Lee, J. Hong, M. Ha, Y.-D. Jung, H. Lim, S.Y. Kim, H. Ko, Giant tunneling piezoresistance of composite elastomers with interlocked microdome arrays for ultrasensitive and multimodal electronic skins, ACS Nano 8 (2014) 4689–4697.
[50] M. Ma, Z. Zhang, Q. Liao, F. Yi, L. Han, G. Zhang, S. Liu, X. Liao, Y. Zhang, Self-powered artificial electronic skin for high-resolution pressure sensing, Nano Energy 32 (2017) 389–396.
[51] Y. Yang, J. Han, J. Huang, J. Sun, Z.L. Wang, S. Seo, Q. Sun, Stretchable energy-harvesting tactile interactive interface with liquid-metal-nanoparticle-based electrodes, Adv. Funct. Mater. 30 (2020), 1909652.
[52] Z. Wen, Y. Yang, N. Sun, G. Li, Y. Liu, C. Chen, J. Shi, L. Xie, H. Jiang, D. Bao, Q. Zhuo, X. Sun, A wrinkled PEDOT:PSS film based stretchable and transparent triboelectric nanogenerator for wearable energy harvesters and active motion sensors, Adv. Funct. Mater. 28 (2018), 1803684.
[53] G. Zhao, Y. Zhang, N. Shi, Z. Liu, X. Zhang, M. Wu, C. Pan, H. Liu, L. Li, Z.L. Wang, Transparent and stretchable triboelectric nanogenerator for self-powered tactile sensing, Nano Energy 59 (2019) 302–310.
[54] Y. Lee, J. Kim, B. Jang, S. Kim, B.K. Sharma, J.-H. Kim, J.-H. Ahn, Graphene-based stretchable/wearable self-powered touch sensor, Nano Energy 62 (2019) 259–267.
[55] X. Pu, Q. Tang, W. Chen, Z. Huang, G. Liu, Q. Zeng, J. Chen, H. Guo, L. Xin, C. Hu, Flexible triboelectric 3D touch pad with unit subdivision structure for effective XY positioning and pressure sensing, Nano Energy 76 (2020), 105047.

Jiahui He received the B.S. degree of Biomedical Engineering from the Jinan University, Guangzhou, in 2019. He is currently pursuing the MPhil degree at the Department of Biomedical Engineering, City University of Hong Kong, China. His research interests mainly include design and fabrication of biomedical sensor and wearable device.

Zhaoqian Xie is a Professor of Engineering Mechanics at Dalian University of Technology in China. He obtained a Bachelor and Ph.D. degrees from Dalian University of Technology in 2006 and 2013, respectively. After working as a postdoctoral fellow in the Departments of Civil and Environmental Engineering at Northwestern University in USA from 2014 to 2019, and Senior Research Fellow in the Departments of Biomedical Engineering at City University of Hong Kong from 2019 to 2020, he joined the Department of Engineering Mechanics at Dalian University of Technology in 2020. His research interests include solid mechanics, experimental mechanics, and wireless communication/energy harvesting of wearable and bio-integrated electronics.

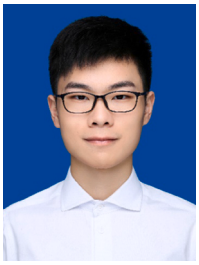

Kuanming Yao is a Ph.D. student in the Department of Biomedical Engineering at the City University of Hong Kong since 2019. He received his Bachelor degree in Zhejiang University in 2019, and then joined Dr. Xinge Yu & Dr. Lidai Wang's research groups. His research interests include triboelectric nanogenerators, flexible electronics, human-machine interface and biomedical imaging techniques.

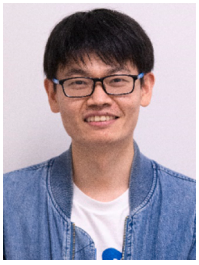

Dengfeng Li is currently a Postdoctoral Fellow in the Department of Biomedical Engineering, City University of Hong Kong. He received his Bachelor degree from Xi'an Jiaotong University, Master degree from Tsinghua University, and the Ph.D. degree from City University of Hong Kong. His research interests include flexible electronics, biomedical device, soft materials, and robotics.

Yiming Liu is a Ph.D. student in the Department of Biomedical Engineering at the City University of Hong Kong since 2018, research assistance in the Department of Architecture and Civil Engineering since 2017. He received his Bachelor degree in Tianjin University in 2015, and his M.Sc. in Hong Kong University of Science and Technology in 2017. His research interests include piezoelectric nanogenerator, triboelectric nanogenerator, flexible electronics, skin-integrated electronics, and wind energy.

Xinge Yu is currently an Assistant Professor of Biomedical Engineering at City University of Hong Kong (CityU). He finished his Ph.D. research of printable flexible electronics at Northwestern University (NU) and University of Electronic Science and Technology of China in 2015. From 2015–2018, Xinge Yu was a postdoc. in the Center for Bio-Integrated Electronics at NU and the Department of Materials Science and Engineering at the University of Illinois at Urbana-Champaign. His research focus on developing skin-integrated electronics and bio-electronics, and conducting multidisciplinary research addressing challenges in biomedical applications.